Supplementary information for "Quantum and classical confinement of resonant states in a trilayer graphene Fabry-Pérot interferometer"

L. C. Campos,[1] A. F. Young,[1] K. Surakitbovorn,[1] K. Watanabe,[2] T. Taniguchi,[2] and P. Jarillo-Herrero[1]

[1]*Department of Physics, Massachusetts Institute of Technology, Cambridge, Massachusetts 02139*

[2]*Advanced Materials Laboratory, National Institute for Materials Science, 1-1 Namiki, Tsukuba 305-0044, Japan.*

Supplementary Figures

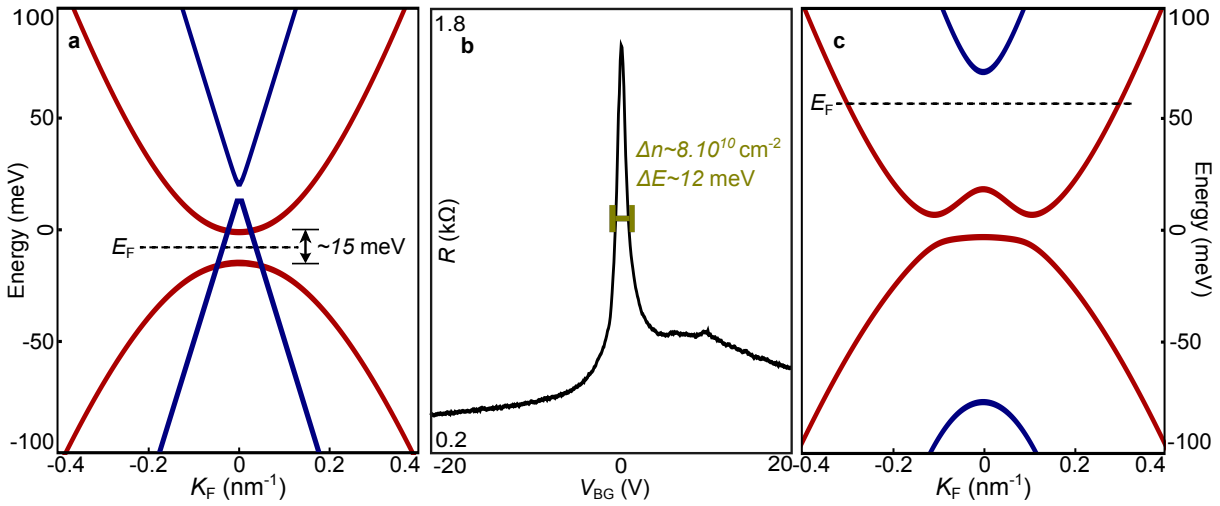

Supplementary Figure S1: Band structure of Bernal stacked (ABA) trilayer graphene. **(a)** Energy band structure at zero transverse electric field ($\Delta_1 = 0$). The ABA TLG bands are composed of a combination of BLG-like subbands (red)and MLG-like subbands (blue). The low energy subbands are composed of offset, overlapping MLG-like and BLG-like bands. While at most energies TLG is a multiband conductor, a small energy window of ∼15 meV exists near charge neutrality in which the hole type MLG-like band is isolated. Trilayer graphene is thus purely MLG-like in a small charge density window of $\Delta n \sim 10^{11}$ cm^{-2}. Accessing this regime is only possible if carrier inhomogeneity over the sample is $n < 10^{11}$ cm^{-2}, necessitating high mobility devices. **(b)** Two terminal resistance data as a function of the $V_{\rm BG}$ at $n_{\rm TG} = 0$, at $T \sim 300$ mK. We estimate the field effect mobility in our device from the Drude model, $\mu = (L^{'}/W)(1/C)dG/dV_{\rm BG}$, where $L^{'}$ is the channel length, W is the channel width, and C is the capacitance per unit area. The estimate gives ($\mu = 60,000$ cm^{2}V^{-1}s^{-1}) close to the charge neutrality point. By measuring the full-width at half-maximum of the resistance peak ($\Delta V_{\rm BG} = 1.2$ V), we estimate a charge carrier inhomogeneity to be $\Delta n \leq 8.10^{10}$ cm^{-2}. We estimate the mean free path of the charge carriers from the formula $\sigma = (2e^2/h)k_{\rm F}l_{\rm mf}$ to be $l_{\rm mf} = 600\ nm$. **(c)** Energy band structure at finite transverse electric field.

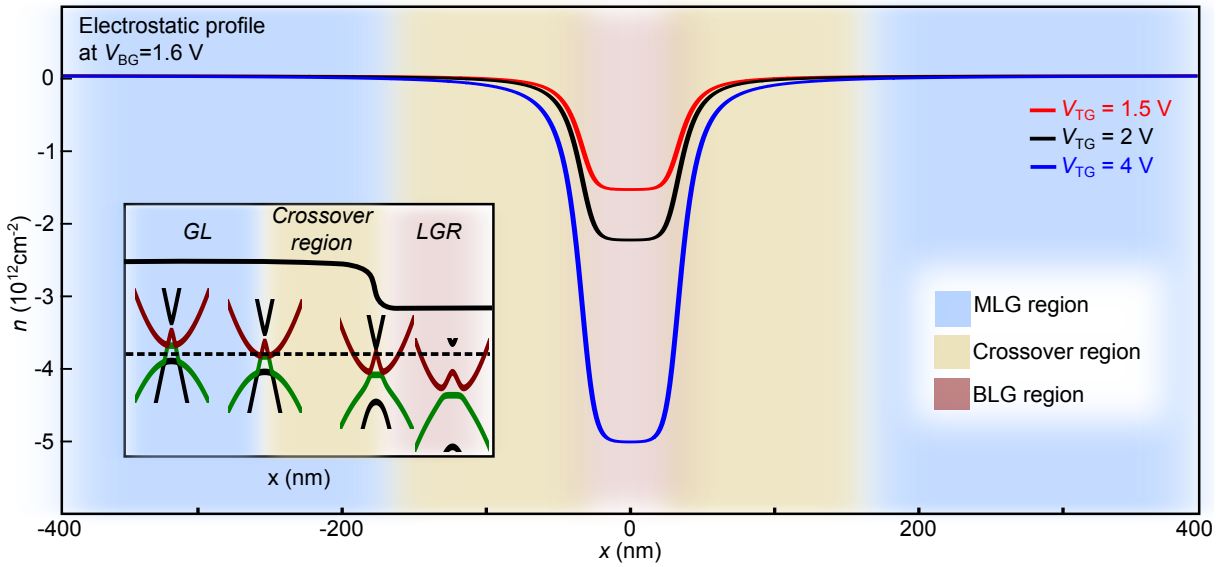

Supplementay Figure S2: Electrostatic profile in the giant oscillation regime for three different values of top gate voltages (V_{TG}). A broad crossover region divides the regions characterized by isolated MLG-like and BLG-like bands. **Inset**, Detail of the crossover region. Deep in the GLs, the charge carriers are purely MLG-like, while in the center of the LGR they are purely BLG-like. In between, fringe fields from the local gate lead to a wide crossover region characterized by multiband transport.

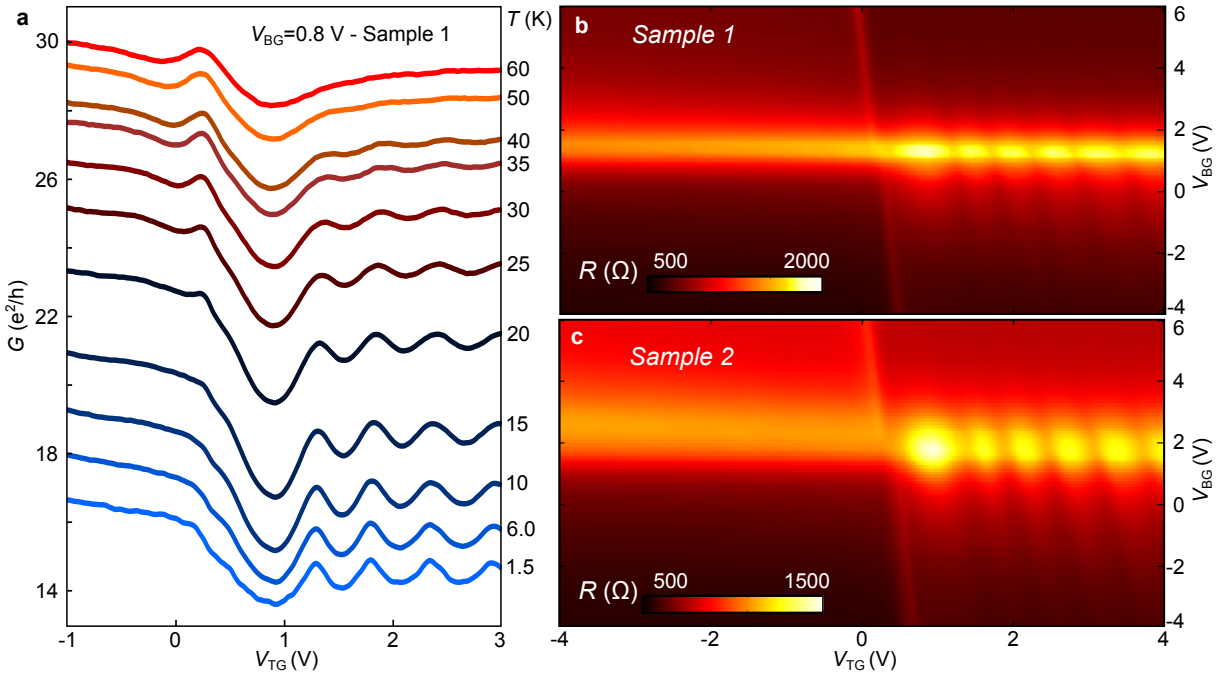

Supplementary Figure S3: Temperature dependence and observation of the giant oscillation in different samples. (a) Temperature dependence of the giant FP oscillations with $V_{\mathrm{BG}} = 0.8$ V ($n_{\mathrm{GLs}} \sim 10^{11}\mathrm{cm}^{-2}$) performed on sample 1. Increasing the temperature increases the conductance of the sample in this regime, simultaneously attenuating the giant oscillations. Both effects are qualitatively consistent with expectations. The insulator-like temperature coefficient suggests thermal activation of GL carriers to the BLG-like conduction and valence bands. The giant oscillations are robust up to temperatures of ∼50 K. This number is roughly consistent with the available energy window for monolayer-type states in the GLs of about 15 meV. A naive estimate would set an upper bound of $T_{\mathrm{MAX}} \sim 15\mathrm{meV}/(2\mathrm{k_B}) = 87$ K. However, disorder likely suppresses this further, by at least 1 meV∼ 10 K (ref. 31). Further calculations are required in order to understand the role of other decoherence processes at finite temperature. **(b)** Observation of the giant FP oscillations at 300 mK on sample 1. **(c)** Observation of the giant FP oscillations at 300 mK on sample 2.

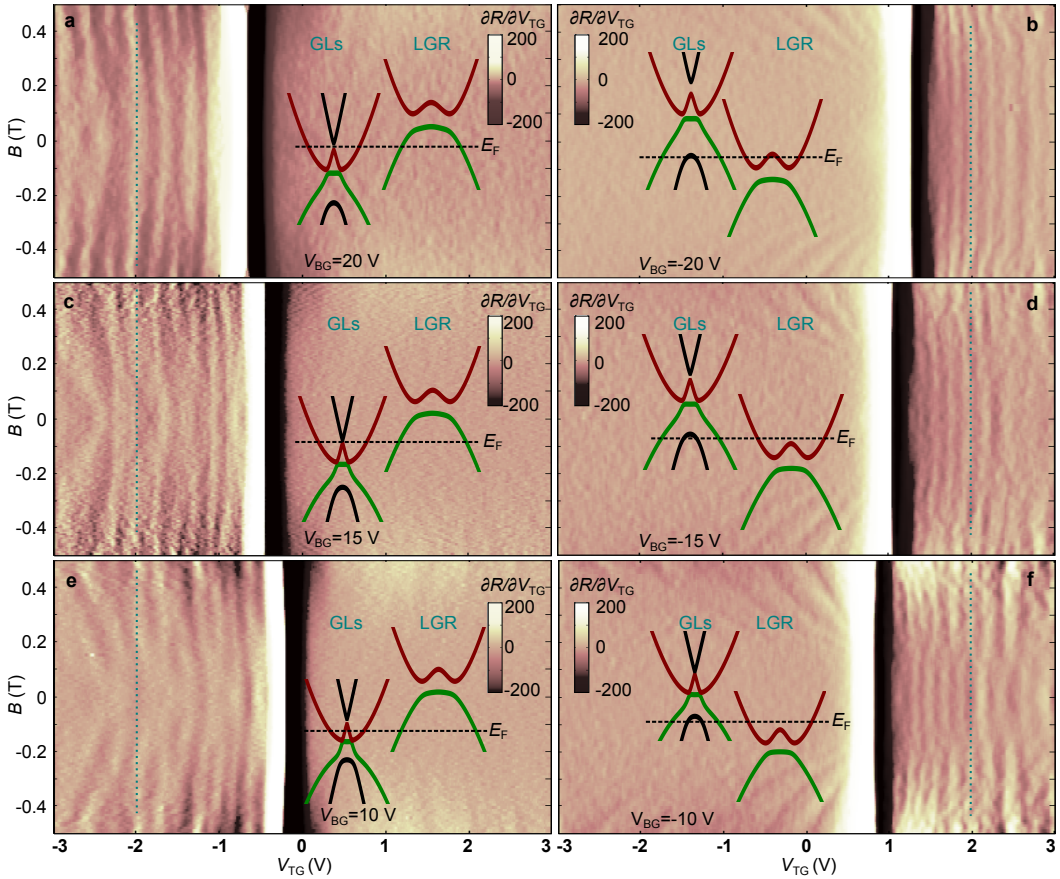

Supplementary Figure S4: **Magnetic field dependence of the small FP oscillations.** Here we plot the derivative of the resistance with respect to V_{TG} for several values of V_{BG}. The inset in each figure depicts the energy band structure of the GLs and LGR states for the value of $V_{\rm TG}$ denoted by the dotted vertical line. Unlike the giant oscillations, the small oscillations observed throughout the ambipolar regions survive in magnetic field, until the eventual crossover to the Shubnikov de Haas regime. These oscillations are associated mostly with transmission through larger $k_{||}$ states, which do not decouple as rapidly. The precise description of the behavior of the small oscillation at low fields is beyond the scope of this paper, but there is a rich phenomenology to be studied arising from the multiband transport and its interplay with chirality. **(a)** $V_{\rm BG} = 20$ V. **(b)** $V_{\rm BG} = -20$ V. **(c)** $V_{\rm BG} = 15$ V. **(d)** $V_{\rm BG} = -15$ V. **(e)** $V_{\rm BG} = 10$ V. **(f)** $V_{\rm BG} = -10$ V. In some cases, such as **f**, there is an apparent π phase shift in the oscillations (at $B{\sim}200$ mT).

Supplementary Discussion

The device electrostatics suggest a natural division of the charge carrying channel into two regions: the graphene leads (GLs) and the locally gated region (LGR). The energy dispersion and carrier density in the GLs is tuned by varying V_{BG}, while the band structure in the LGR is dependent on the combination of V_{BG} and V_{TG}. To precisely describe the energy bands and carrier density throughout the sample, we simulate the electric field profile over the sample using the commercial Comsol Multiphysics software package (see Supplementary Figure S2). For the electrostatics simulations, we take the trilayer to be a perfect conductor, and fit the dielectric constant of the hBN ($\varepsilon \simeq 3.2$) to match the voltages corresponding to charge neutrality in the LGR, given experimentally measured (by AFM) hBN thicknesses. We calculate the applied electric field, and resulting Δ_1, as a function of distance along the channel. Supplementary Figure S1c shows the band structure of the LGR under the local gate when $V_{\mathrm{TG}} = 3$ V and $V_{\mathrm{BG}} = 1.6$ V ($|D| = 0.35$ V/nm), for which the Fermi level in the LGR lies in a BLG-like subband. The spatial profile of the band structure and displacement field are then input into the calculations of the transmission probabilities, described in the next section.

In our simulations, we neglect the effects of quantum capacitance (C_Q). In the graphene leads, the channel is gated only by the back gate. Even at the low GL densities where the giant oscillations are observed, the C_Q is at least 80 times larger than the geometrical capacitance of the back gate, C_{BG}. The resulting correction to the total capacitance, $C^{-1} = C_{BG}^{-1} + C_Q^{-1}$, is of order 1%. The locally gated region is gated both by the top gate and back gate. The geometric capacitance of the top gate, $C_{TG} \gg C_{BG}$, potentially leading to a larger correction; however, in the giant oscillation regime, the density—and correspondingly, the density of states and by extension C_Q—in the LGR is much larger than the density in the GLs (this essentially happens because the Fermi energy is tuned well into the BLG-like band). Thus even under the top gate, the quantum capacitance is never less than $\sim$30 times larger than C_{TG}, giving a maximum correction to the density profile of order 3%. Incorporating such a small effect is well beyond the scope of our simplified model for the trilayer graphene band structure.

Fabry-Perot oscillations and the transmission probability through the pn interface. Conductance oscillations in ballistic electronic Fabry-Pérot interferometers can be

modeled using a phase coherent Landauer formula[32]:

$$G_{\mathrm{pnp}} = \frac{4e^2}{h} \sum_{k_\parallel} \left| \frac{T_- T_+ e^{-L_{\mathrm{LGR}}/2l_{\mathrm{mf}}}}{1 - R_- R_+ e^{i\theta} e^{-L_{\mathrm{LGR}}/l_{\mathrm{mf}}}} \right|^2 \tag{S1}$$

Here, θ is the phase accumulated as particles cross the electrostatically induced Fabry-Pérot cavity,

$$\theta = 2\mathrm{Re}\left\{ \frac{1}{\hbar} \int_-^+ p_{\mathrm{x}}(x')dx' \right\} \tag{S2}$$

$T_\pm$ and $R_\pm$ denote the transmission and reflection amplitudes at the first (+) and second (−) pn junction. In the main text, we assume $T_+ = T_- = T$, which is valid in the absence of a magnetic field and neglecting trigonal warping.

As discussed in the main text, both semiclassical and quantum effects contribute to the ballistic transport properties of graphene etalons. The semiclassical contribution, T_{SC}, arises from the translation symmetry of the electrostatic potential, which leads to conservation of momentum parallel to the symmetric barrier, $k_\parallel$. Whenever the Fermi momentum is decreasing as a function of coordinate, states with $|k_{\mathrm{F}}| < |k_\parallel|$ are transmitted only evanescently, leading to an exponential suppression of T. In monolayer graphene, k_F vanishes at the center of a pn junction, leading to exponentially preferred reflection of all obliquely incident carriers (ref. 33).

$$T_{\mathrm{SC}} = e^{-Im\left\{\frac{1}{\hbar}\int_-^+ p_{\mathrm{x}}(x')dx'\right\}} \tag{S3}$$

Chiral particles also receive a major contribution from pseudospin matrix elements[33–36], denoted by T_{Q}.

$$T_{\mathrm{Q}} = |\langle \Psi_{\mathrm{GL}} | \Psi_{\mathrm{LGR}} \rangle| \tag{S4}$$

The total transmission amplitude through a single pn junction can be approximated by the product of these two effects,

$$T = T_{\mathrm{SC}} \cdot T_{\mathrm{Q}} \tag{S5}$$

Device electrostatics. Supplementary Figure S2 shows the electrostatic profile along the device in the giant oscillation regime, $V_{\mathrm{BG}} = 1.6$ V and $V_{\mathrm{TG}} > 0$. In this regime, the GL Fermi level lies in the isolated MLG-like band, while the LGR Fermi level lies in the isolated BLG-like electron band (see inset in Supplementary Figure S2). While the

electrostatic interface is quite sharp ($\lesssim$10 nm, comparable to the hBN thickness), the band structure crossover region, in which there is a coexistence of a MLG-like and BLG-like bands, penetrates far ($\sim$150 nm) into the GLs. This wide crossover region is a consequence of the interplay between the electric fields from the top and bottom gates, which simultaneously modulate the band structure and doping.

At zero magnetic field, the boundaries of the Fabry-Perot interferometer coincide with the electrostatic potential sharp step. This is because the density and band structure in the crossover region change adiabatically: eigenstates of the Hamiltonian at coordinate x are very similar to eigenstates of the Hamiltonian at coordinate $x + \delta x$, and incident particles in the MLG-like band have a very low probability of scattering to the BLG-like band. In contrast, at the edge of the top gate, the large displacement field gradient leads to a sudden change in the electronic structure, and induces interband matrix elements. The oscillations at zero magnetic field are dominated by the quantum transmission probability for interband scattering; consequently, the distance between the density steps is the appropriate choice for describing the size of the FP cavity. This is borne out by the fitting of the oscillation period (see Figure 3a of the main text), which shows a good match when this distance L_{LGR}=78 nm, is chosen.

However, the smooth crossover region plays an important role in carrier collimation, and consequently the magnetic field induced suppression of the giant oscillations. The classical decoupling induced by a magnetic field is a consequence of momentum conservation: particles that accumulate more than a certain $k_{\|}$ in the central region cannot propagate in the GLs, where k_{F} is small, and decouple from transport. Above a certain value of B, this applies to all states contributing to the giant oscillations at $B = 0$. This implies that the relevant length for the classical decoupling is defined by the distance between the two MLG-like/crossover region boundaries: for a particle in a BLG-like state in the LGR, deconfinement from the LGR is always possible through interband transitions, but momentum conservation prohibits the particle escaping beyond the edge of the crossover region. This is confirmed by the data, where a match to the theory is found for a B_{C} with $L \sim$360 nm.

Supplementary Methods

ABA Energy Band Structure. The electronic structure of Bernal stacked or ABA trilayer graphene (TLG) consists of both monolayer and bilayer graphene (MLG and BLG)-like electronic bands[37,38]. Starting from the usual sublattice basis, the ABA TLG Hamiltonian can be transformed via a unitary transformation into a quasi-block diagonal form composed of MLG-like (H_m) and BLG-like (H_b) blocks[37],

$$H = \begin{pmatrix} H_m & U \\ U^T & H_b \end{pmatrix}, U = \begin{pmatrix} \Delta_1 & 0 & 0 & 0 \\ 0 & 0 & 0 & \Delta_1 \end{pmatrix} \tag{S6}$$

$$H_m = \begin{pmatrix} \Delta_2 - \gamma_2/2 & \upsilon\pi^\dagger \\ \upsilon\pi & \Delta_2 - \gamma_5/2 + \delta \end{pmatrix} \tag{S7}$$

$$H_b = \begin{pmatrix} \Delta_2 + \gamma_2/2 & \sqrt{2}\upsilon_3\pi & -\sqrt{2}\upsilon_4\pi^\dagger & \upsilon\pi^\dagger \\ \sqrt{2}\upsilon_3\pi_\dagger & -2\Delta_2 & \upsilon\pi & -\sqrt{2}\upsilon_4\pi \\ -\sqrt{2}\upsilon_4\pi & \upsilon\pi^\dagger & -2\Delta_2 + \delta & \sqrt{2}\gamma_1 \\ \upsilon\pi & -\sqrt{2}\upsilon_4\pi^\dagger & \sqrt{2}\gamma_1 & \Delta 2 + \gamma_5/2 + \delta \end{pmatrix} \tag{S8}$$

The off-diagonal block U vanishes for zero interlayer asymmetry. A transverse electric field induces an energy difference between adjacent layers[37] (Δ_1), coupling the diagonal blocks and causing hybridization of the energy bands.

In our band structure calculations, we numerically solve the ABA Hamiltonian as a function of the applied electric field. The input parameters consist of the electric field profile, calculated from finite element analysis, and the Slonczewski-Weiss-McClure parameters (SWMcC), taken from the values recently obtained from analysis of Landau level crossings in TLG[38] (see table below). The operator $\pi = \xi p_x + i p_y$, where $\xi = \pm 1$ for the dispersion around the $K(K')$ valley. The SWMcC paramters are used to calculate the effective velocities parameterizing Eq. S8 (ref. 37), $\upsilon = (\sqrt{3}/2)a\gamma_0/\hbar$, $\upsilon_3 = (\sqrt{3}/2)a\gamma_3/\hbar$, and $\upsilon_4 = (\sqrt{3}/2)a\gamma_4/\hbar$.

SWMcC parameters

γ_0	γ_1	γ_2	γ_3	γ_4	γ_5	δ
3.1 eV	0.39 eV	-0.028 eV	0.315 eV	0.041 eV	0.05 eV	0.046 eV

For simplicity, we take the energy difference between the central graphene layer and the average of the outer layers to be zero ($\Delta_2 = 0$), and approximate the energy difference between adjacent layers (Δ_1) as a linear function of the applied electric field. Following reference 39, we take the screening of the average displacement field, $D = (D_{\mathrm{BG}} + D_{\mathrm{TG}})/2$, to be 40%, giving $\Delta_1 = -0.6edD$ where e is the fundamental charge, and d is the inter layer separation (0.34 nm).

Supplementary References

[31] Xue, J. *et al.* Scanning tunnelling microscopy and spectroscopy of ultra-flat graphene on hexagonal boron nitride. *Nat Mater* **10**, 282–285 (2011).

[32] Young, A. F. & Kim, P. Electronic transport in graphene heterostructures. *Annu. Rev. Condens. Matter Phys.* **2**, 101–120 (2011).

[33] Cheianov, V. V. & Fal'ko, V. I. Selective transmission of dirac electrons and ballistic magnetoresistance of n-p junctions in graphene. *Phys. Rev. B* **74**, 041403 (2006).

[34] Katsnelson, M. I., Novoselov, K. S. & Geim, A. K. Chiral tunnelling and the klein paradox in graphene. *Nat Phys* **2**, 620–625 (2006).

[35] Allain, P. & Fuchs, J. Klein tunneling in graphene: optics with massless electrons. *The European Physical Journal B - Condensed Matter and Complex Systems* **83**, 301–317 (2011).

[36] Gu, N., Rudner, M. & Levitov, L. Chirality-assisted electronic cloaking of confined states in bilayer graphene. *Phys. Rev. Lett.* **107**, 156603 (2011).

[37] Koshino, M. & McCann, E. Gate-induced interlayer asymmetry in aba-stacked trilayer graphene. *Phys. Rev. B* **79**, 125443 (2009).

[38] Taychatanapat, T., Watanabe, K., Taniguchi, T. & Jarillo-Herrero, P. Quantum hall effect and landau-level crossing of dirac fermions in trilayer graphene. *Nat Phys* **7**, 621–625 (2011).

[39] Koshino, M. Interlayer screening effect in graphene multilayers with aba and abc stacking. *Phys. Rev. B* **81**, 125304 (2010).